Advances in Concrete Construction, *Vol. 10, No. 3 (2020) 195-209*
DOI: https://doi.org/10.12989/acc.2020.10.3.195

Effectiveness of steel fibers in ultra-high-performance fiber-reinforced concrete construction

Behrooz Dadmand[1a], Masoud Pourbaba[2b], Hamed Sadaghian[3c] and Amir Mirmiran[*4]

[1]Department of Civil Engineering, Razi University, Kermanshah, Iran
[2]Department of Civil Engineering, Maragheh Branch, Islamic Azad University, Maragheh, Iran
[3]Department of Civil Engineering, University of Tabriz, Tabriz, Iran
[4]Department of Civil Engineering, University of Texas at Tyler, Tyler, TX, USA

(*Received June 1, 2020, Revised July 10, 2020, Accepted August 5, 2020*)

Abstract. This study investigates the behavior of ultra-high-performance fiber-reinforced concrete (UHPFRC) with hybrid macro-micro steel and macro steel-polypropylene (PP) fibers. Compression, direct and indirect tension tests were carried out on cubic and cylindrical, dogbone and prismatic specimens, respectively. Three types of macro steel fibers, i.e., round crimped (RC), crimped (C), and hooked (H) were combined with micro steel (MS) and PP fibers in overall ratios of 2% by volume. Additionally, numerical analyses were performed to validate the test results. Parameters studied included, fracture energy, tensile strength, compressive strength, flexural strength, and residual strength. Tests showed that replacing PP fibers with MS significantly improves all parameters particularly flexural strength (17.38 MPa compared to 37.71 MPa). Additionally, the adopted numerical approach successfully captured the flexural load-deflection response of experimental beams. Lastly, the proposed regression model for the flexural load-deflection curve compared very well with experimental results, as evidenced by its coefficient of correlation (R^2) of over 0.90.

Keywords: fiber reinforced concrete; high/ultra-high performance concrete; steel fiber reinforced concrete (SFRC); hybrid reinforcement; modeling

1. Introduction

Advancements in concrete technology have brought forth a new class of cementitious materials known as ultra-high-performance concrete (UHPC), with low water-to-cementitious materials ratio and high compressive strength. The drawback of UHPC is its brittleness, which may be addressed by adding fibers to improve tensile strength, deformation capacity, durability, and toughness. The exceptional characteristics of ultra-high-performance fiber-reinforced concrete (UHPFRC) in comparison to conventional concrete make it a very good choice for long-span bridges and high-rise buildings (Swamy, 1985) and in recent many attempts have been made to characterize the behavior of fiber-reinforced concrete (FRC) both experimentally and numerically in various conditions (Aslani *et al.* 2014a, b, Aslani *et al.* 2015, Mazloom *et al.* 2020, Mansouri *et al.* 2020, Raj *et al.* 2020, Kandekar *et al.* 2020). Various types of fibers such as natural, metallic, and polymeric, e.g., polypropylene (PP) may be used in UHPFRC (Brandt, 2005)

Single fibers, commonly used in most concrete materials (Yoo *et al.* 2017a), are only efficient up to a certain limit, and typically improve either strength or ductility (Banthia and Gupta, 2004). High-strength fibers such as steel, glass, and carbon mainly contribute to the strength, with insignificant effects on ductility. In contrast, PP and nylon fibers are low in strength, but improve ductility quite effectively (Soe *et al.* 2013, Halvaei *et al.* 2016).

Researchers have also used hybrid fibers for a more holistic improvement in the behavior of concrete (Sharma and Bansal 2019, Ganesan *et al.* 2017, Sridhar and Parsad, 2019). This study aims at assessing the performance of hybrid steel- and steel-PP fiber-reinforced UHPCs through extensive tests on different types of specimens, with a contribution to the rather limited datasets on hybrid UHPFRCs.

2. State of knowledge on hybrid FRCs

2.1 Hybrid steel fiber-reinforced UHPC

Kim *et al.* (2011) investigated the flexural behavior of micro and macro fiber-reinforced hybrid UHPCs. Macro smooth fiber ($\frac{l_f}{d_f}=\frac{30}{0.3}$), macro end-hooked (H) fiber A ($\frac{l_f}{d_f}=\frac{30}{0.375}$), macro H fiber B ($\frac{l_f}{d_f}=\frac{62}{0.775}$), macro twisted

*Corresponding author, Professor
E-mail: amirmiran@uttyler.edu
[a]MSc.
E-mail: b.dadmand@gmail.com
[b]Assistant Professor
E-mail: pourbaba@iau-maragheh.ac.ir
[c]MSc.
E-mail: sadaghian.hamed@gmail.com

http://www.techno-press.org/?journal=acc&subpage=7
ISSN: 2287-5301 (Print), 2287-531X (Online)

fiber ($\frac{l_f}{d_f} = \frac{30}{0.3}$) and micro-smooth fiber ($\frac{l_f}{d_f} = \frac{13}{0.2}$) in ratios of 0.5%, 1.0%, 1.5% and 2.0% were used, respectively where l_f and d_f were the length and diameter of fibers in mm. Four-point bending tests on prismatic beams based on ASTM C1609 (2012) showed hybrid UHPFRCs to perform much better than their single micro UHPFRC counterparts both in terms of deflection and energy absorption. As compared to the UHPFRC specimen with only 2% micro fibers, blending micro and macro fibers in equal volumetric ratios increased deflection and toughness corresponding to the modulus of rupture (MOR) stress by at least 45% and 49%, respectively.

Park *et al*. (2012) investigated the tensile behavior of hybrid UHPFRCs with combined 1% (by volume) of different types of macro steel fibers (long smooth, two types of H fibers and twisted) with varying dosages of smooth MS fibers. Results showed that the overall shape of the stress-strain curve is mainly influenced by the type of macro fibers, while micro fibers improve strength and multiple-cracking behavior. With respect to the post-peak cracking, strain capacity and multiple-cracking behavior, specimens with twisted fibers had the best performance, while those with long smooth fibers had the worst performance.

Direct tension stress-strain response of hybrid UHPFRC specimens with different sizes and geometries was investigated by Nguyen *et al*. (2014) using 1% macro twisted and 1% micro smooth steel fibers. Their assessment of geometric parameters (e.g., gauge length, cross-sectional area, volume, and thickness) revealed considerable effects on strain capacity, energy absorption and multiple-cracking behavior, but a negligible influence on post-peak strength. All parameters decreased with an increase in gauge length, cross-sectional area and volume of UHPFRC. Increased thickness led to higher strain capacity and energy absorption, whereas different width-to-thickness ratios yielded opposite trends in size effects.

Wu *et al*. (2016) studied uniaxial compression stress-strain behavior, cracking pattern and toughness of prismatic UHPFRC specimens with 6 and 13 mm long hybrid steel fibers and an overall ratio of 2% by volume. Results showed that UHPFRC with 1.5% long and 0.5% short fibers had the best compressive response, with 34% increase in strength, 46% increase in strain at peak stress, and 22% increase in modulus of elasticity, compared to UHPC. The worst behavior was reported for singly-reinforced UHPC with 2% short fibers.

The impact of basalt, polyvinyl-alcohol, and polyethylene in various fiber proportions up to 1.5% by volume were studied by Kang *et al.* (2016) through a series of compression, tension, and density tests. The hybrid system comprised of steel fibers and one of the above-mentioned fibers. They reported that adding synthetic fibers generally improves tensile strength but not the compressive strength of UHPFRC. They further noted that adding microfibers would not create any unintentional pore.

Flexural performance of single and hybrid steel UHPFRCs was assessed by Yoo *et al*. (2017b); using H, twisted and medium straight fibers in overall ratios of 2% by volume. For the hybrid type, a portion of H and twisted fibers were replaced with medium straight fibers (0.5% and 1.5% by volume). They noted that single short steel fibers exhibited the best performance in terms of deflection capacity, toughness, and cracking behavior. Single twisted fibers with 2% fiber ratios performed better than hybrid use of twisted fibers and medium-length straight steel fibers in ratios of 0.5% and 1.5%, respectively. However, hybrid use of 1% twisted and 1% medium-length straight steel fiber proved to be as good as the twisted fibers with 2% fiber content. For the same fiber content, short steel fibers, owing to their better distribution, showed higher compressive strength than both H and twisted fibers.

Effects of fiber hybridization on the flexural behavior of UHPFRC was studied by Yoo *et al*. (2017c) using short (13 mm), medium (19.5 mm) and long (30 mm) steel fibers at various fractions. Short fibers had a better flexural performance than long fibers, but not as good as medium-length fibers. Hybrid use of long and medium-length fibers improved the toughness, fiber bridging capacity and cracking behavior.

2.2 Hybrid PP fiber-reinforced FRC and UHPFRC

Although numerous research can be found in the literature regarding the hybrid use of steel and PP fibers in FRCs, few studies exist with regard to their hybrid use in UHPFRCs, as discussed below:

Hsie (2008) reported a considerable improvement in compressive strength, splitting tensile strength and MOR with the use of a hybrid coarse monofilament. Tests also demonstrated staple PP fibers to easily distribute in the mix due to their fineness.

Sahoo *et al*. (2014) tested seven full-scale hybrid FRC beams in flexure, with steel and PP fibers in ratios of 0.5% and 1% by volume. They noted that the mere addition of PP fibers had no effect on either compressive or splitting tensile strength, while significantly improving ductility (by 120%), post-peak and multiple-cracking behavior. It was also observed that fiber ratios in excess of 0.5% do not contribute to the flexural resistance of the beam.

Xu *et al*. (2016) studied the tensile behavior of hybrid steel-PP FRCs using dogbone specimens with 19 mm long PP fibers in ratios of 0.11% to 0.19%, and steel fibers in lengths of 13.5 to 36 mm and dosages of 1.1% to 1.9%. Fibers improved tensile strength by 25% to 80%, with steel fiber contributing to the peak strength and PP fibers to the residual strength.

Smarzewski (2017) studied the behavior of hybrid steel-PP UHPFRCs under different curing periods. Parameters such as absorbability, apparent density, open porosity, compressive strength, MOR were assessed at 28, 56 and 730 days. Results showed that increasing the PP content would reduce density by as much as 11% while increasing absorption up to 33%. Increasing steel content showed a similar effect, in addition to increasing density. Longer curing periods improved the mechanical properties of concrete, due to delayed hydration and improved adhesion properties.

Şanal (2018) fabricated seven mixes using different proportions of steel fiber fly ash and macro synthetic PP fibers. Tests on both H- and PP-FRCs showed that

Table 1 Mix proportions (Pourbaba *et al*. 2018a, b, 2019a, b)

Material	Proportion by weight (%)
Cement	28.04
Fine sand	39.95
Silica fume	9.22
Quartz powder	8.35
Superplasticizer	1.20
Fiber	6.00
Water	7.24

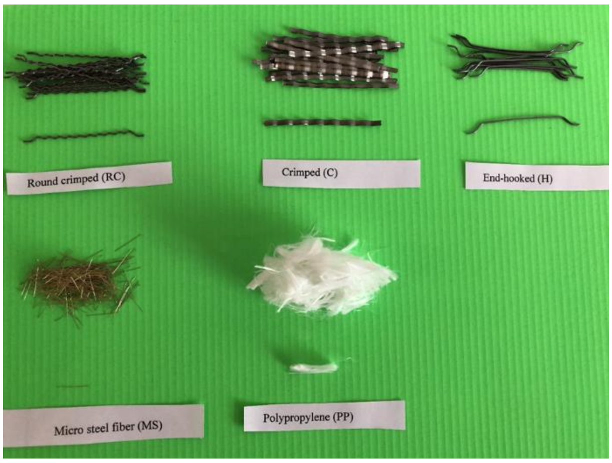

Fig. 1 Steel and PP fibers used in this study

increasing fiber content would reduce compressive strength, with 0.8% PP fibers proving to be as effective as 1% H fibers. H fibers increased preserved water, while PP fibers helped reduce water absorption.

Li *et al*. (2018) studied the flexural behavior of hybrid FRCs with steel fibers (straight, H and corrugated) in various lengths and dosages, combined with monofilament PP fibers. Synergetic effects were noted for all types of hybrid systems, mainly for pre-peak rather than post-peak regions. The increase in steel and PP ratios led to increased ductility and flexural strength. Steel fibers played a major role in increasing flexural strength. The best synergy was observed in hybrid straight and PP fibers, while hybrid systems with H and MS fibers had the highest and lowest compressive and split tensile strengths, respectively.

3. Experimental program

3.1 Materials and mix design

The implemented composition of the mix was based on previous studies by the authors according to Table 1 (Pourbaba *et al.* 2018a, b, Pourbaba *et al.* 2019a, b). According to the requirements of ASTM C150/C150M (2017), type II Portland Cement, superplasticizer, water, fine sand with a maximum diameter of 1.1 mm, silica fume and quartz powder were used. Round crimped (RC), Crimped (C), and H fibers were mixed with MS and PP fibers in overall ratios of 2% by volume. It is noteworthy that PP fibers are low in density and therefore their relative mass yields higher volumes in the mix. Fig. 1 shows the

Table 2 Chemical composition of cementitious materials

Composition (% mass)	Proportion by weight (%)
CaO	64.59
Al_2O_3	5.71
SiO_2	21.13
Fe_2O_3	3.00
MgO	1.27
SO_3	2.70
Loss on ignition	1.6

Table 3 Specifications of steel and PP fibers

Fiber ID	Type of fiber	Density (g/cm^3)	Diameter/ Width, *d* (mm)	Length, *l* (mm)	Tensile strength (MPa)	Modulus of elasticity (GPa)
RC	Round crimped	7.80	0.850	30	2000	200
C	Crimped	7.80	0.750	30	1800	200
H	End-hooked	7.80	0.760	30	1900	200
MS	Micro steel	7.80	0.160	13	2700	200
PP	Polypropylene	0.91	0.048	15	400	6.9

types of fibers used in the study. Table 2 shows the chemical composition of the concrete mix and Table 3 details the properties of fibers. It should be noted that the content of fibers was distributed evenly among different mixes to get a homogenous mix. Based on the fiber type, six mixes were cast in which RC1%, C1%, and H1% were blended with PP1% and MS1%. The number following the fiber types denotes the proportion of the fiber by volume in the mix.

3.2 Mechanical tests

Compression tests were carried out on 100×100×100 mm^3 cubes and 100×200 mm^2 cylinders with at least three specimens tested for each mix in each mechanical test. Loading was applied at a rate of 0.2 MPa/s. Moduli of elasticity (E_c) tests were also conducted on 100×200 mm^2 cylinders (ASTM 469/469M, 2014), with LVDTs recording the data according to the setup presented in Fig, 2(a) and the modulus of elasticity calculated as follows:

$$E_c = \frac{0.4f_c' - f_{c1}}{\varepsilon_2 - 0.00005} \tag{1}$$

where f_c' is the cylindrical compressive strength of UHPFRC, f_{c1} is the stress corresponding to a strain of 5×10^{-6}, and ε_2 is the strain corresponding to $0.4f_c'$. Direct tension tests were carried out on dogbone specimens, with a larger section at the grips, gradually tapering to 45×55 mm at the critical mid-section. The load was applied in a displacement-controlled manner at a rate of 0.01 mm/s. Dimensions of the specimens are shown in Figs. 2(b) and 2(c), respectively. Lastly, four-point bending tests were carried out on 100×100×450 mm prismatic beams ((Fig. 2(d)). Loading was applied in a displacement-controlled manner at a rate of 1 mm/min LVDTs were used to monitor the deflection values at mid-span.

4. Numerical analyses

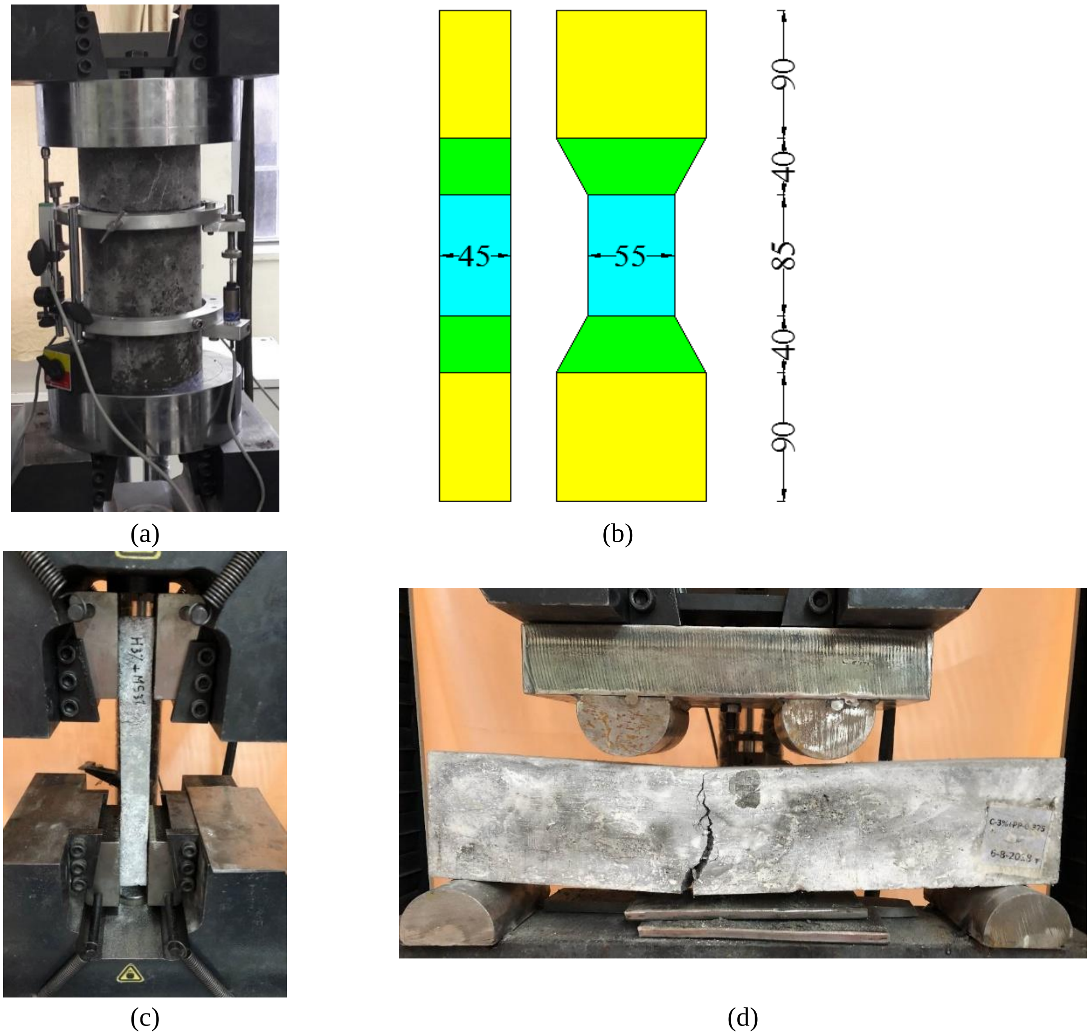

Fig. 2 Dimensions and test setup: (a) modulus of elasticity, (b) dogbone specimen, and (c) direct tension test setup (d) flexural test setup (unit: mm)

4.1 Introduction

The objective of the analysis is to identify correct parameters to capture the flexural response of UHPFRC according to the developers of ATENA (2016), software in which analyses are carried out. Tensile parameters are the most critical properties, which may be directly used in a numerical simulation, or can be estimated, based on the accuracy of the methodology used, via inverse analyses of bending tests (Mezquida-Alcar 2019). On the other hand, characterization of the tensile response via the indirect method poses some challenges, i.e., several calibrations of key parameters from each indirect test are required to capture the direct tension stress vs. crack width response which inevitably introduce statistical uncertainty and sophistication to indirect tests that can be easily avoided by carrying out direct tension tests. In this study, ATENA (2016) was used together with the GID (2015) preprocessor to simulate the flexural response of UHPFRC. The software has in the past been used for ordinary concrete (Farzam and Sadaghian 2018, Farzam *et al.* 2019, Sadaghian and Farzam 2019, Rasoolinejad and Bažant 2019) and FRC (Kannam and Sarella 2018).

4.2 Materials, mesh and solution methods

In this study, a fracture-plastic model was used that combines the constitutive model for tensile (fracturing) and compressive (plastic) behavior (ATENA 2016). Compressive strengths, moduli of elasticity and tensile strengths obtained from test results were used as input parameters. 20-mm thick steel plates with a linear behavior were used to simulate loading plates and pinned supports. Eight-noded 3D hexahedral elements were used to mesh the loading plates, supports, and the concrete beam. The load was applied in a displacement- controlled manner at a rate of 0.1 mm/sec. Corresponding load values at the two loading plates and mid-span deflection were monitored. The Newton-Raphson method was used to solve the equations. It is noteworthy that in the fracture model, the response of a crack is defined by the traction-separation relationship, i.e., tensile function. A crack, despite being considered a displacement discontinuity, is able to transfer stress between its faces, which subsequently, through a traction-separation relationship, is related to the crack opening displacement. In this regard, to obtain reasonable results the crack band model was used and to reduce the mesh

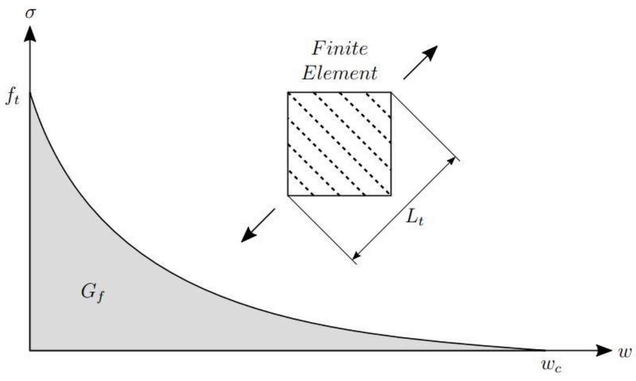

(a)

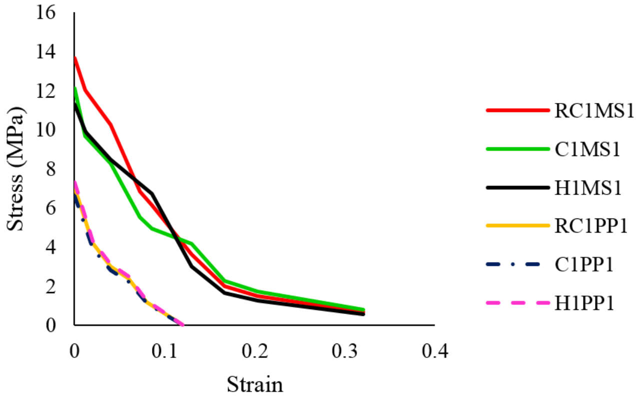

(b)

Fig. 3 Tensile parameters for the tensile function (a) schematic tensile softening and definition of L_t (ATENA 2016), (b) tensile function curves for numerical analyses

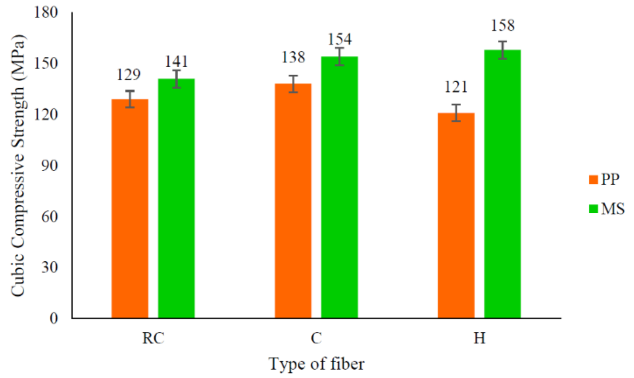

(a)

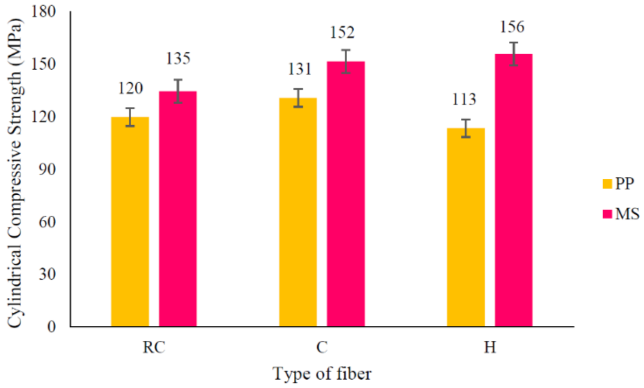

(b)

Fig. 4 Cubic and cylindrical compressive strengths (a) cubic, (b) cylindrical

dependency, the band width (characteristic length, L_t) and the element size were related to one another (ATENA, 2016). L_t is a material parameter, which should be equal to the element size. The fracture strain used in the tensile function is defined as

$$\varepsilon = \frac{w}{L_t} \tag{2}$$

where ε is the fracture strain; w is the crack width and L_t is the characteristic length defined in Fig. 3(a). The tensile function used for each beam type is shown in Fig. 3(b). It is worth mentioning that the tensile functions of hybrid PP fibers are almost independent of the fiber and the only difference is in the tensile strengths which shift the curve a bit. Besides, high strain values up to 0.3 with low-stress values for hybrid steel fibers have been considered to avoid numerical stabilities where severe cracking occurs in the strain localization branch. As discussed above, the most important parameters to be considered are as follows:

Tensile function, which is the primary parameter for UHPFRC. This curve is a measure of ductility in tension, which also shows the evolution of post-peak tensile stresses. Steps to simulate the behavior of fiber-reinforced composites are as follows:

- Input tensile strength and the tensile function, the abscissa of which is the fracture strain and its ordinate is the tensile stress after tensile strength is reached.
- Perform the analysis, export the load-deflection curves monitored at their respective locations and compare them with their experimental counterparts.
- If the difference between the two graphs is satisfactory, the model is acceptable. Otherwise, fracture strains should be determined at deflections with significant differences as per Eq. (2). Using the initial tensile function and linear interpolation, stress values at calculated fracture strain should be adjusted proportionally to test results. It should be noted that the number of required modifications is contingent upon the accuracy desired by the user.

5. Results and discussions

5.1 Behavior in compression

Figs. 4(a) and 4(b) show the cubic and cylindrical compressive strengths, respectively. It is observed that the combination of macro fibers with the micro MS fiber yields higher compressive strengths than their combination with the PP fiber. This is justifiable since micro fibers prevent the propagation of fine crack and that the tensile strength and stiffness of MS fibers are well greater than that of PP fibers. After the formation of initial cracks, macro fibers resist against the widening of the cracks by bridging between macro cracks until slippage occurs.

The highest difference in replacement of the PP fiber with MS fiber was observed in H fibers as H1MS1 showed

Table 4 Available equations in the literature for the modulus of elasticity of UHPFRC

Researcher(s)	Equations (unit: MPa)	Note	RC1MS1	C1MS1	H1MS1	RC1PP1	C1PP1	H1PP1
Kollmorgen (2004)	$E_c = 11800(f_c')^{\frac{1}{3.14}}$	$34 \le f_c' \le 207$ MPa	56.22	58.39	58.90	54.18	55.70	53.24
KCI (2007)	$E_c = 8500\sqrt[3]{f_c' + 8}$	---	44.40	46.10	46.50	42.82	44.00	42.09
Graybeal (2007)	$E_c = 3840\sqrt{f_c'}$	$126 \le f_c' \le 193$ MPa	44.54	47.28	47.92	---	43.91	---
Graybeal and Stone (2012)	$E_c = 4069\sqrt{f_c'}$	$97 \le f_c' \le 179$ MPa	46.93	49.81	50.49	44.29	46.26	43.09
Alsalman *et al.* (2017)	$E_c = 8010(f_c')^{0.36}$	$31 \le f_c' \le 235$ MPa	46.78	48.83	49.31	44.87	46.29	43.99
Haber *et al.* (2018)	$E_c = 3755\sqrt{f_c'}$	$64.8 \le f_c' \le 153$ MPa	43.56	46.23	46.86	41.10	42.93	39.99
Current study	---	---	49.37	50.44	47.36	40.09	39.14	39.40

Table 5 Ratios of predicted to experimental values of moduli of elasticity

Specimen	Experimental E_c (GPa)	$\frac{E_{c,Kollmorgen}}{E_{c,exp.}}$	$\frac{E_{c,KCI}}{E_{c,exp.}}$	$\frac{E_{c,Graybeal}}{E_{c,exp.}}$	$\frac{E_{c,Graybeal\,\&\,Stone}}{E_{c,exp.}}$	$\frac{E_{c,Alsalman\ et\ al.}}{E_{c,exp.}}$	$\frac{E_{c,Haber\ et\ el.}}{E_{c,exp.}}$
RC1MS1	49.37	1.14	0.90	0.90	0.95	0.95	0.88
C1MS1	50.44	1.16	0.91	0.94	0.99	0.97	0.92
H1MS1	47.36	1.24	0.98	1.01	1.07	1.04	0.99
RC1PP1	40.09	1.35	1.07	---	1.10	1.12	1.03
C1PP1	39.14	1.42	1.12	1.12	1.18	1.18	1.10
H1PP1	39.4	1.35	1.07	---	1.09	1.12	1.02

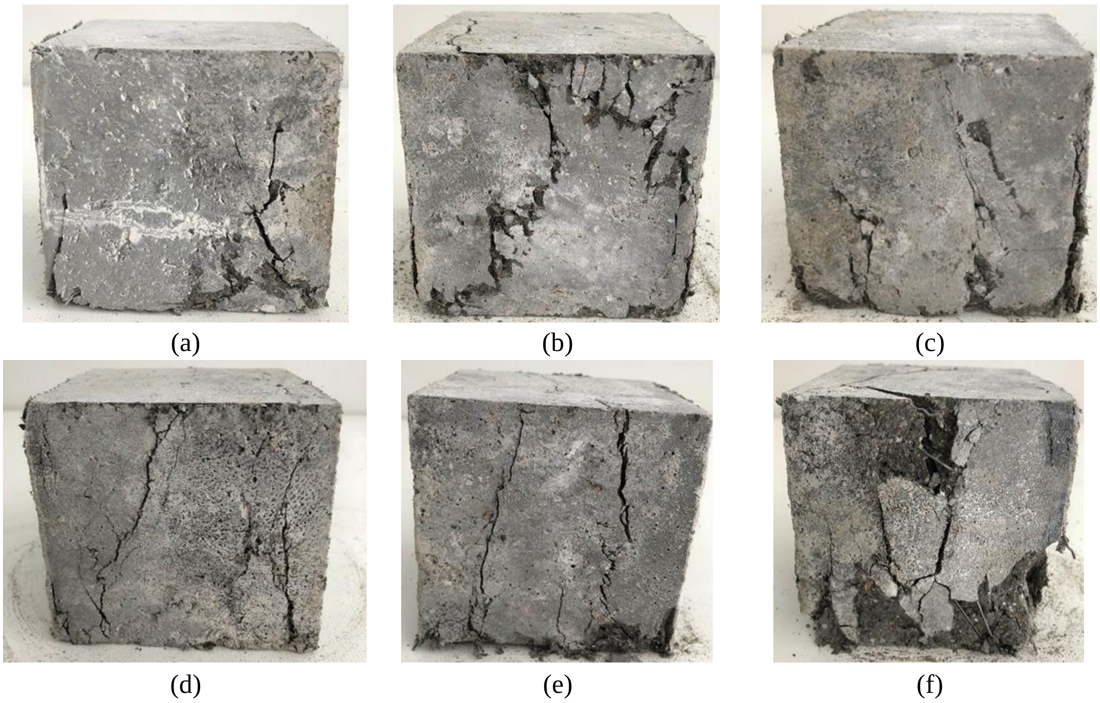

Fig. 5 Crack pattern of cube specimens: (a) RC1MS1, (b) C1MS1, (c) H1MS1, (d) RC1PP1, (e) C1PP1, and (f) H1PP1

23% higher strength compared to H1PP1 and the lowest difference was for the RC fiber where RC1MS1 gave 10% higher strength than RC1PP1; similar trends were also observed for the cylindrical specimens. It was expected that, owing to the larger diameter of the RC fiber in comparison to the H fiber, hybrid combinations containing RC fibers would yield higher compressive strengths in comparison to their H fiber counterparts. However, it is hypothesized that the sinusoidal shape of the RC fiber has a weaker bond with the concrete matrix in compression than the H fiber with hooked ends and slips, therefore yielding lower compressive strength than the H-fiber combinations. Among hybrid steel fibers, the difference between compressive strengths was negligible (less than 10%) and for their PP counterparts, the difference was not significant. Furthermore, comparison of cubic and cylindrical specimens show that the conversion factor between two compressive strengths approach unity with the increase in compressive strength i.e., the conversion factor lies between 0.9289 for the RC1PP1 with a cubic compressive strength of 129 MPa and 0.9857 for the H1MS1 specimen with a cubic compressive strength of 158 MPa. Lastly, it should be added that moduli of elasticity values for RC1PP1 and H1PP1 according to the equation proposed by Graybeal

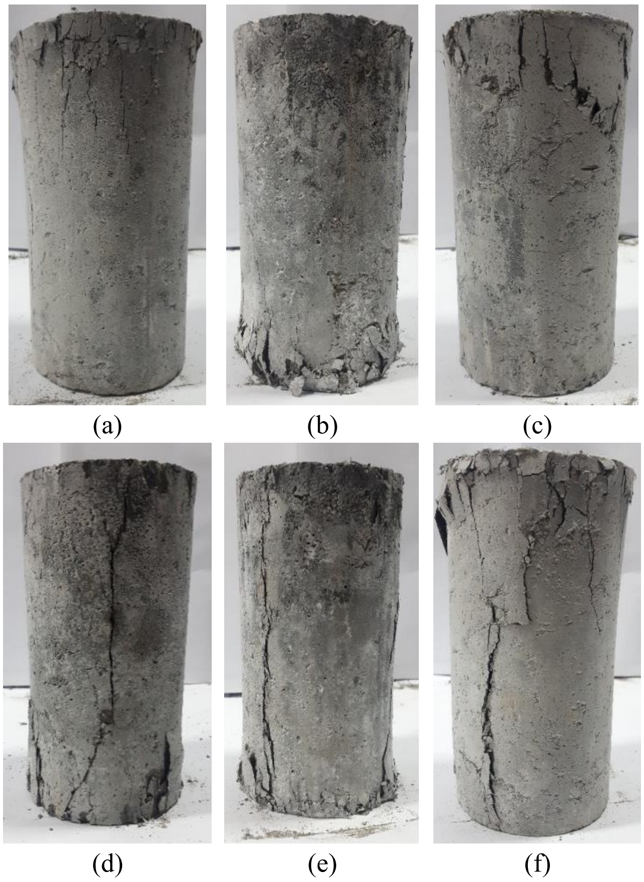

Fig. 6 Crack pattern of cylindrical specimens: (a) RC1MS1, (b) C1MS1, (c) H1MS1, (d) RC1PP1, (e) C1PP1, and (f) H1PP1

(2007) have not been given in Tables 4 and 5 since their cylindrical compressive strengths do not fall within the range stipulated by Graybeal (2007).

5.2 Cracking pattern in cubes and cylinders

Figs. 5 and 6 show crack patterns of cubic and cylindrical specimens, respectively. All cubic specimens preserved their integrity up to failure, without any complete separation and no particular trend was observed in the cracking pattern of cubic specimens. In cylindrical specimens, hybrid steel specimens underwent compressive axial forces which were characterized by crushing of concrete at its bottom part or the top regions of the cylinder where the load was applied; in hybrid PP specimens, cracking pattern was somewhat different as longitudinal cracks along the height of the cylinders were formed with wider cracks in comparison to hybrid steel fiber specimens.

5.3 Modulus of elasticity

Stress-strain curves for the determination of modulus of elasticity reveals that almost linear trend governs the behavior (Fig. 7) with hybrid combination of macro and PP fibers giving values between 39.40 GPa and 40.09 GPa while the hybrid combination of macro and micro fibers gave values falling within the 47.36 and 50.44 GPa indicating

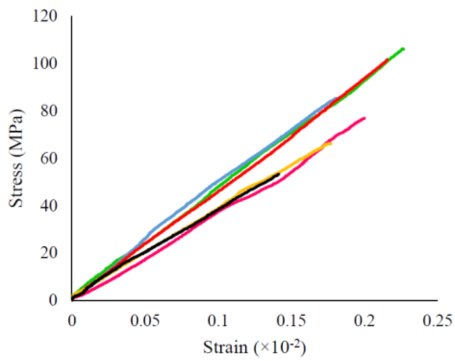

Fig. 7 Stress-strain curves for the determination of modulus of elasticity

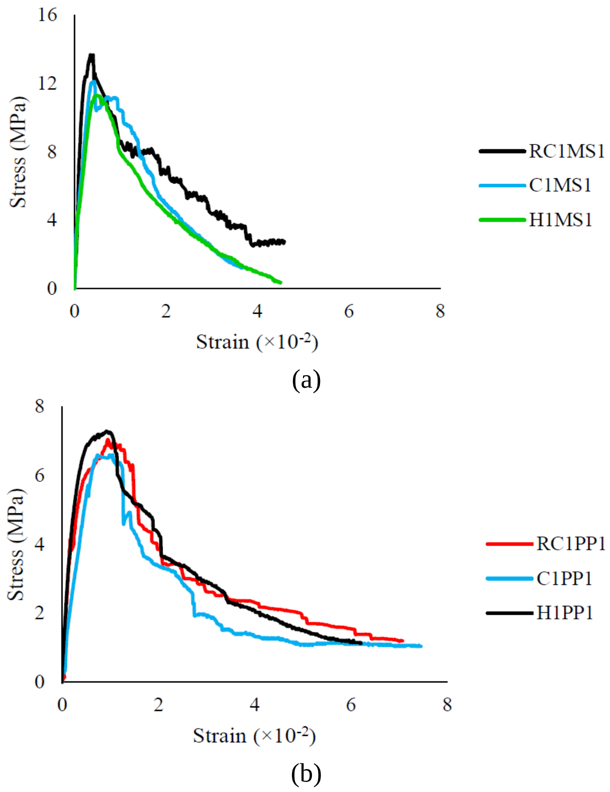

Fig. 8 Stress-strain curves of dogbone specimens (a) hybrid steel fibers, (b) hybrid steel-PP fiber

higher stiffness of micro steel fibers. Additionally, comparison of the experimental moduli of elasticity with available equations. in the literature (Tables 4 and 5) shows that the equation proposed by Kollmorgen (2004), regardless of the type of specimen, overestimates modulus of elasticity especially in those containing PP fibers with the extent of overestimation being as high as 42% for C1PP1. This may be justifiable by the fairly extensive range for the compressive strength that the proposed Eq. covers which in turn means different classes of concrete with notable distinct features and hence the estimation deviates significantly in some cases. For other equations given in the literature the margin of error is mostly less than 15% and mainly underestimate the modulus of elasticity of hybrid steel fibers and overestimate (up to 18% for the C1PP1 specimen) that of the hybrid steel-PP fibers.

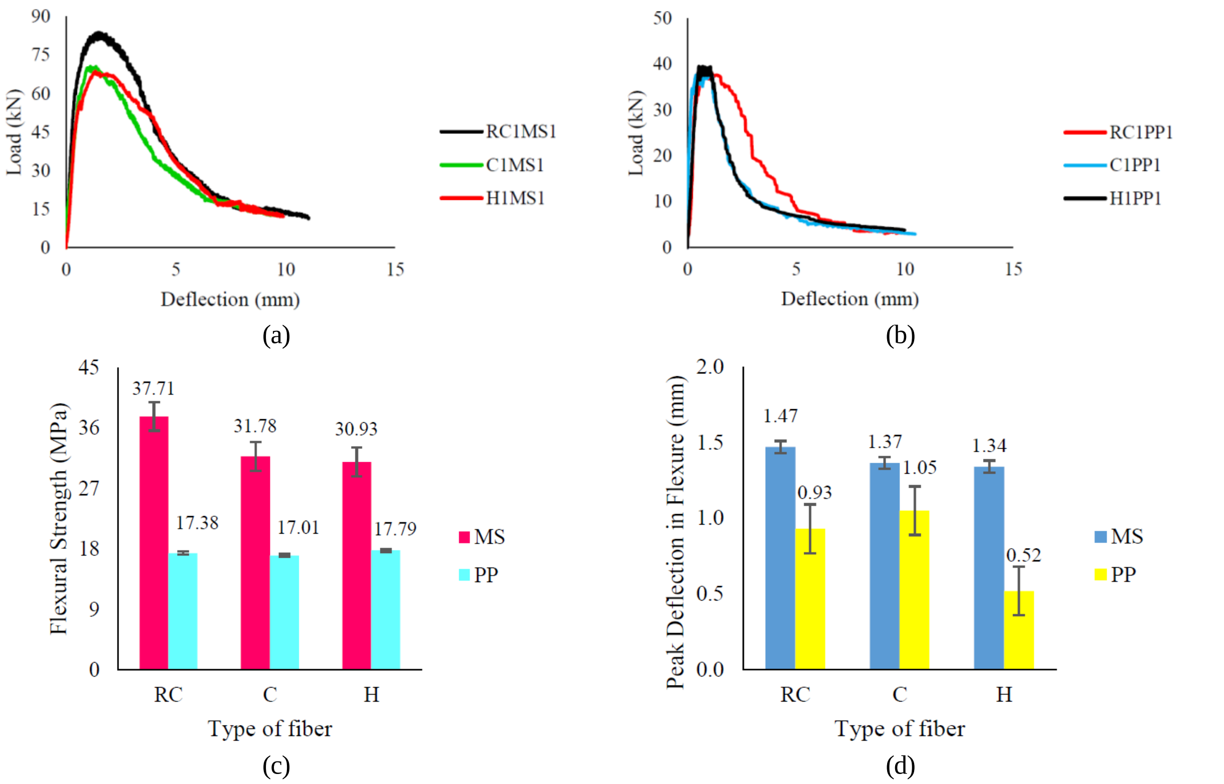

Fig. 9 Flexural load-deflection results: (a) hybrid steel beams (b) hybrid steel-PP beam, (c) flexural strengths, and (d) peak deflections

5.4 Behavior in tension

Fig. 8 shows stress-strain curves of dogbone specimens. As clear from test results, the effect of replacing PP with MS fibers was more pronounced in tension than compression; RC1MS1 specimens had the highest tensile strength (13.68 MPa), which may be attributed to the high tensile strength and aspect ratio of RC fibers which delay the formation of macro cracks, followed by C1MS1 (12.1MPa) and H1MS1 (11.3 MPa) specimens. These values are 94%, 83% and 55% greater than their PP counterparts, a significant difference. It seems that the overall length of the RC fibers, if stretched to become completely straight, is greater than that of C and H fibers and hence, in contrast to what was mentioned in Section 5.1., RC fiber has a better bond with the concrete matrix in tension than C and H fibers that, when combined with the high tensile strength of micro fibers, bring about higher tensile strengths. Concerning stress-strain curves, the shape and overall trend of curves are similar for the two classes of specimens except that in hybrid specimens with PP fibers, larger strain values (at least 6×10^{-2} compared to that of steel fibers (4×10^{-2}) were observed.

5.5 Behavior in flexure

All beams failed in a similar manner, with cracks initiating at mid-span, propagating upwards at higher loads. Replacing PP with MS fibers had its most pronounced effect in flexure, Based on the results, the same concept for the bond between concrete mix and fibers in tension seems to apply to flexure with flexural strengths of up to 37.7 MPa, 31.78 MPa, and 30.93 MPa for RC1MS1, C1MS1, and H1MS1 obtained respectively as compared to their PP counterparts with values equal to 17.38 MPa, 17 MPa, and 17.79 MPa (Figs. 9(a)-9(c)). RC fibers due to their higher tensile and aspect ratio have yielded higher flexural strengths. On the other hand, ultimate deflection seemed independent of the type of hybrid. Lastly, deflection at the peak load is notably higher (ranging from 30% to 157% higher) in the hybrid steel-steel specimens, as compared to steel-PP specimens (Fig. 9(d)).

5.6 Fracture energy in beams

Fig. 10(a) shows steel-steel fiber hybrid systems lead to significantly higher values of toughness (which is defined as the area under the load-deflection curve and serves as a criterion of energy-absorption capacity) at MOR (3.65, 2.01, and 5.66 times higher in RC1MS1, C1MS1, H1MS1, respectively compared to their PP counterparts). A similar trend for toughness is noted at all other deflection values (Figs. 10(b)-10(e). It should be noted that the difference at L/600 is very low, primarily because it falls within the linear portion of the load-deflection curves, hence not much influenced by fiber type. Toughness factor (JSCE 1984) as calculated below (Eq. (3)), further shows the better performance of steel-steel hybrid systems in terms of toughness (Fig. 10(f))

$$TF = \frac{A_{(\frac{L}{150})} L}{\delta_{(L/150)} b h^2} \tag{3}$$

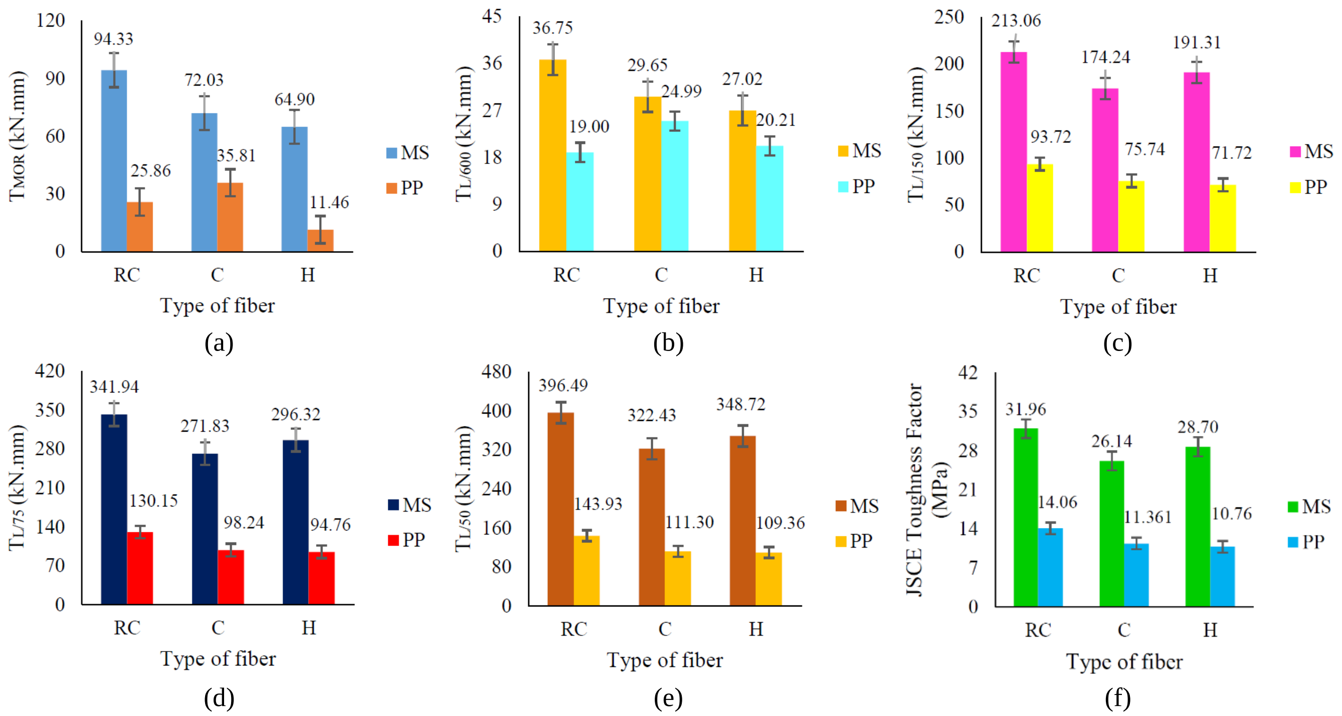

Fig. 10 Toughness values of beam specimens at various deflection points: (a) MOR, (b) L/600, (c) L/150, (d) L/75, (e) L/50, and (f) according to JSCE (1984) at L/150

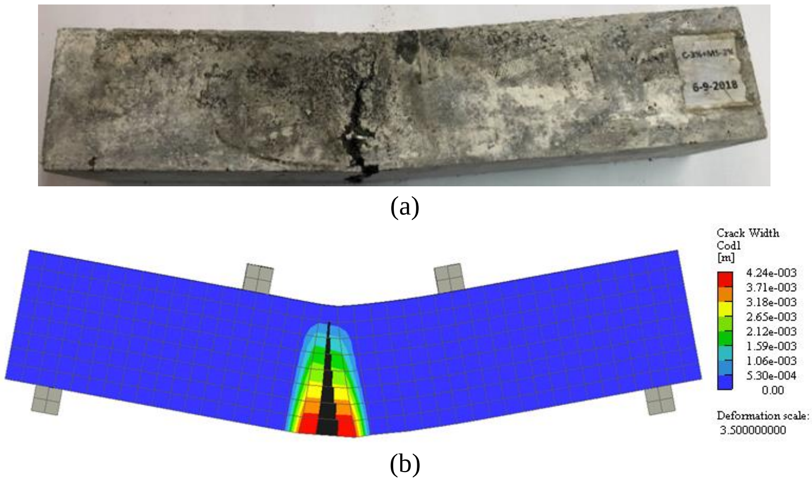

Fig. 11 Typical crack pattern of a hybrid beam (a) experimental (b) numerical (Note: only the main crack has been shown)

where TF = toughness factor; $A_{(L/150)}$= toughness value up to $L/150$; $\delta_{(L/150)}$=3 mm; b and h = width and height of the beam, respectively. A comparison of $T_{L/150}$ proposed by ASTM C1609 (2012) with $T_{L/50}$, shows that $L/150$ is not a good indicator of end deflection point for toughness values. Differences of at least 82% and 47% were observed for hybrid systems with MS and PP fibers, respectively.

5.7 Analytical results and mesh sensitivity

Figs. 11 (a) and 11(b) show the experimental and numerical results for the C1MS1 beam specimen. It can be seen that the crack pattern is quite consistent with the test results. It should be noted that the initial mesh size was equal to 0.0125 m (i.e., 8 elements over the height of the beam). The load-deflection curves presented in Figs. 12(a)-12(f) show good consistency between tests and the model. To verify that further refinement of the mesh is not needed, mesh sensitivity analyses were carried out with 6 and 10 elements over the beam height as well. It can be noted that finer mesh leads to a slightly stiffer response, albeit negligible (Fig. 12(c)).

5.8 Correlation of residual strengths

With regards to residual strengths calculated using ASTM C1609 (2012), i.e., f_{600}^{D} and f_{150}^{D}, which are stresses at $L/600$ and $L/150$, a linear trend is noted (Fig. 13). Values for f_{600}^{D} of hybrid steel fibers were 1.93, 1.72,

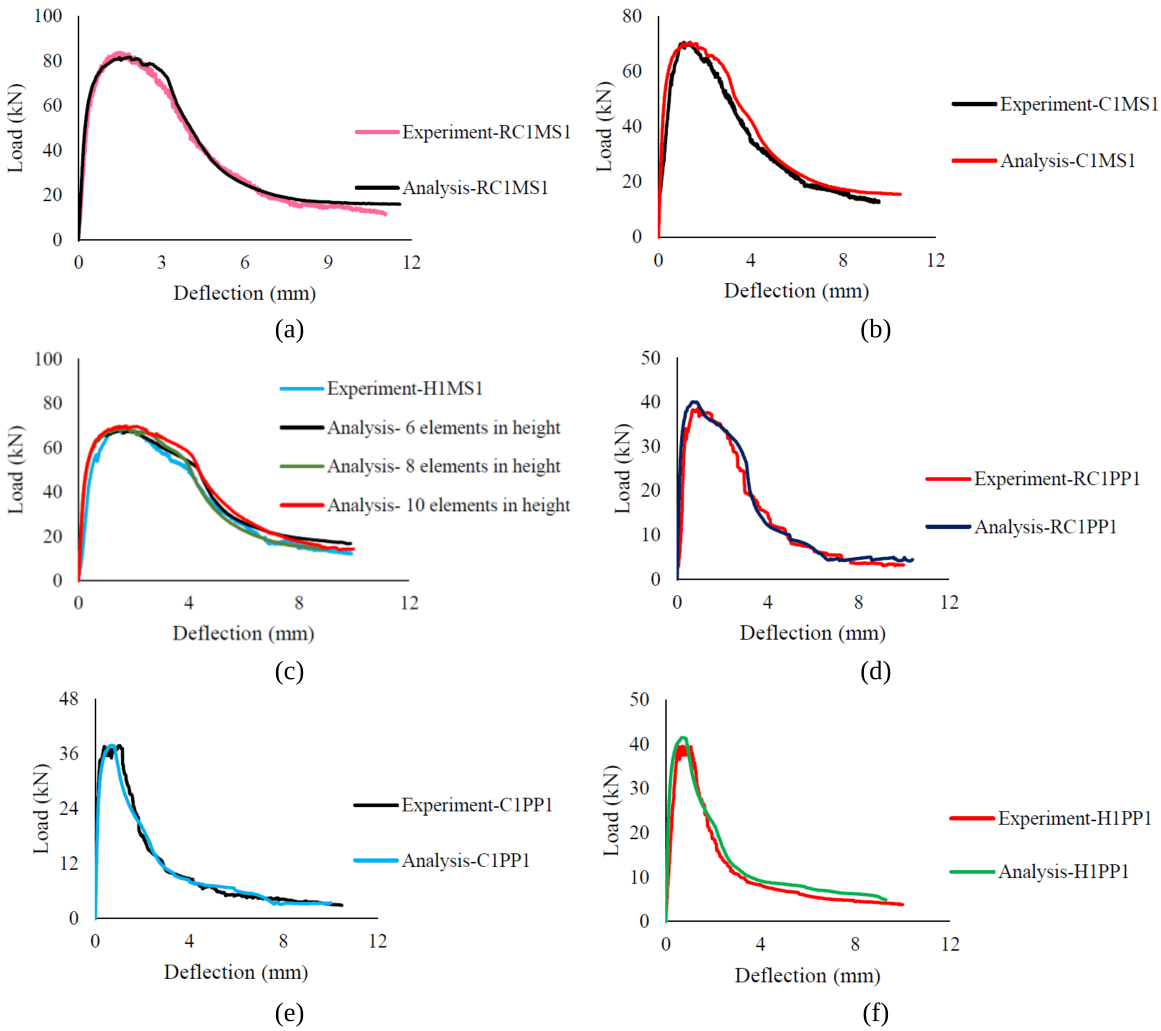

Fig. 12 Comparison of experimental and numerical load-deflection curves (a) RC1MS1, (b) C1MS1, (c) H1MS1, (d) RC1PP1, (e) C1PP1, and (d) H1PP1

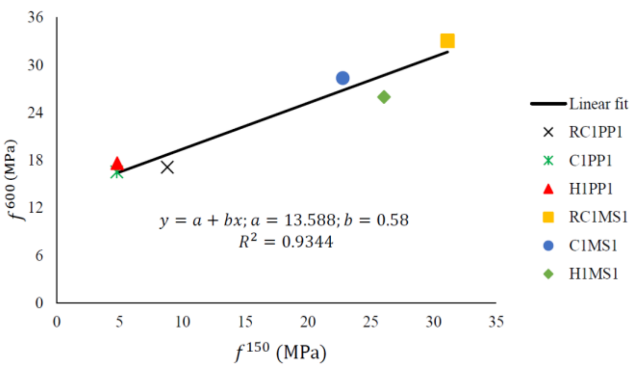

Fig. 13 Correlation of residual strengths in ASTM C1609 (2012)

and 1.47 times higher than their hybrid-PP counterparts and this trend applied also to f_{150}^{D} with values equal to 3.53, 4.75, and 5.41 times higher for RC1MS1, C1MS1, and H1MS1, respectively.

5.9 Fitting of load-deflection curves

It was observed in previous sections that the typical trend of load-deflection curves is characterized by an almost linear increase of load with deflection followed by a descending post-peak branch until failure. Based on the available literature (Yan 2005, Zhenghai 1997), the following conditions apply to a normalized flexural load-deflection curve:

(1) when $x = 0, y = 0$;

(2) for x between zero and unity, the slope of the ascending part is negative;

(3) at peak load x and y are equal to unity and the slope of the curve is equal to zero;

(4) when $x > 1$ and the second derivative with respect to x is equal to zero, it is an inflection point at the descending part;

(5) when $x > 1$ and the third derivative with respect to x is equal to zero, it is where the maximum curvature occurs in the descending branch;

(6) as x approaches infinity, y approaches infinity as well and the slope of the curve approaches zero;

(7) when $x \geq 0$, $0 \leq y \leq 1$.

The model proposed by Wang and Xu (2002) was assessed by Wee *et al*. (1996) and it was reported that it yields favorable results (Eq. (4))

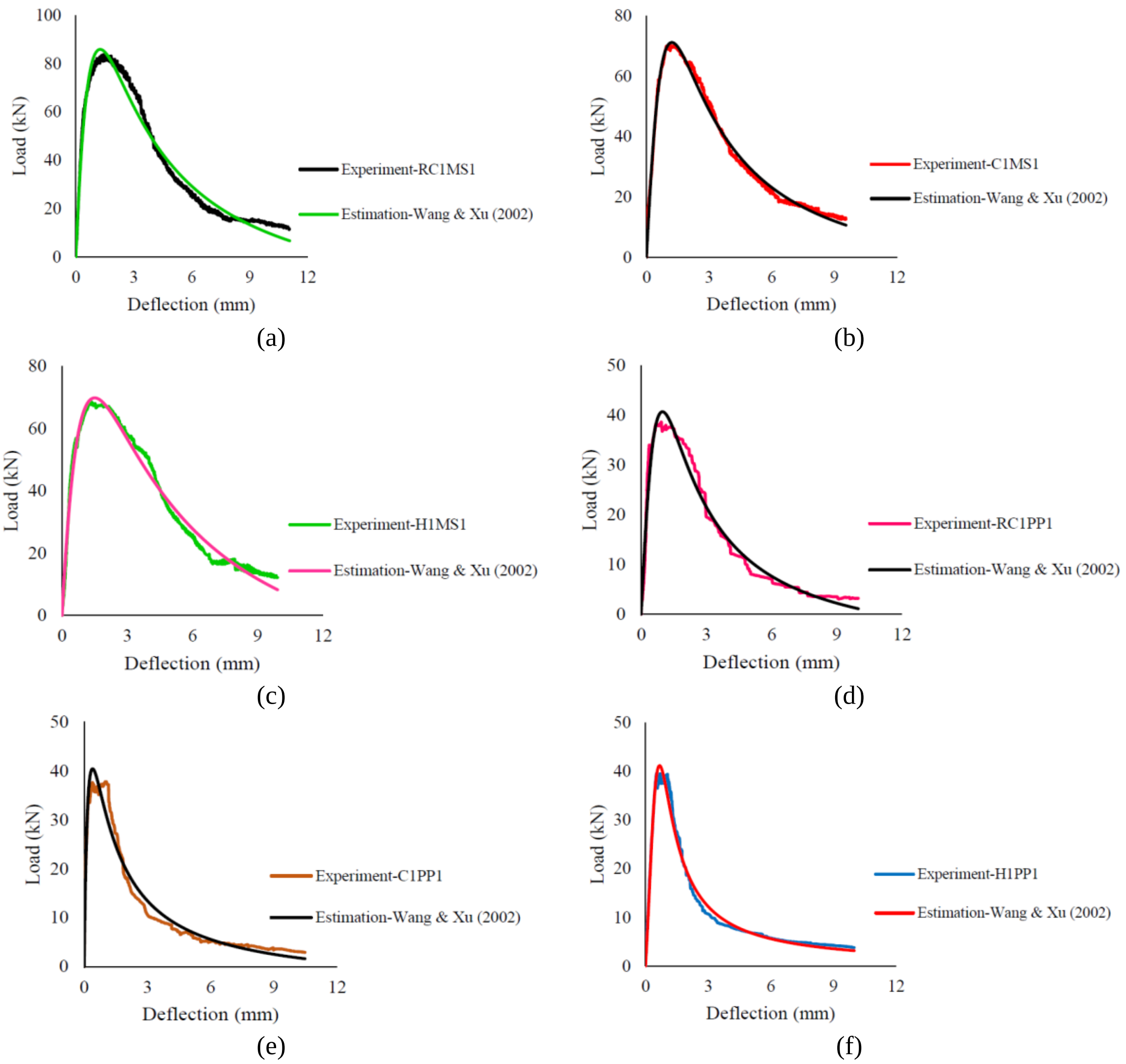

Fig. 14 Fitting curves of beam specimens based on direct fitting based on the work by Wang and Xu (2002) (a) RC1MS1, (b) C1MS1, (c) H1MS1, (d) RC1PP1 (e) C1PP1, and (d) H1PP1

$$y = \frac{ax+bx^2}{1+cx+dx^2} \tag{4}$$

where a, b, c and d are unknown parameters obtained from regression analyses. Wu *et al.* (2016) using the characteristics of the load-deflection curve, and the uniaxial features of concrete in compression given by Wang *et al.* (1978), proposed Eqs. (5) and (6)

Ascending branch

$$y = \frac{Ax-x^2}{1+(A-2)x} \quad 0 \leq x \leq 1 \tag{5}$$

Descending branch

$$y = \frac{x}{B(x-1)^2+x} \quad x > 1 \tag{6}$$

where x is the ratio of a given deflection to its corresponding value at the peak load; y is the ratio of a given load value to the peak load and A and B are fitting parameters. Fitting load-deflection curves and values of fitting parameters for the work by Wang and Xu (2002) and Wu *et al.* (2016) are given in Figs. 14 and 15 and Table 6, respectively. It should be noted that despite the good correlation of the curves (high values of R^2), the model proposed by Wang and Xu (2002) is directly fitted to the experimental curve, making the physical meaning of the parameters unclear.

Based on the obtained experimental load-deflection curves, an equation is proposed for their overall trend based on nonlinear regression analyses as follows

$$y = \frac{a+bx}{1+cx+dx^2} \tag{7}$$

where x and y are defined similar to Eqs. (5) and (6) and a, b, c and d are fitting parameters. The following condition should be met in this Eq. (1) for any value of x or fitting parameters, $y \geq 0$. If otherwise was the case, assume $y = 0$.

It should be noted that Eq. (7) is fitted to experimental curves in two cases (1) one-step application where Eq. (7) is applied to the whole trend of the experimental flexural curves in a single regression (2) two-step application where Eq. (7) is considered for the ascending and descending branch separately. It can be seen that the two-step application of Eq. (7) yields better results than the one-step

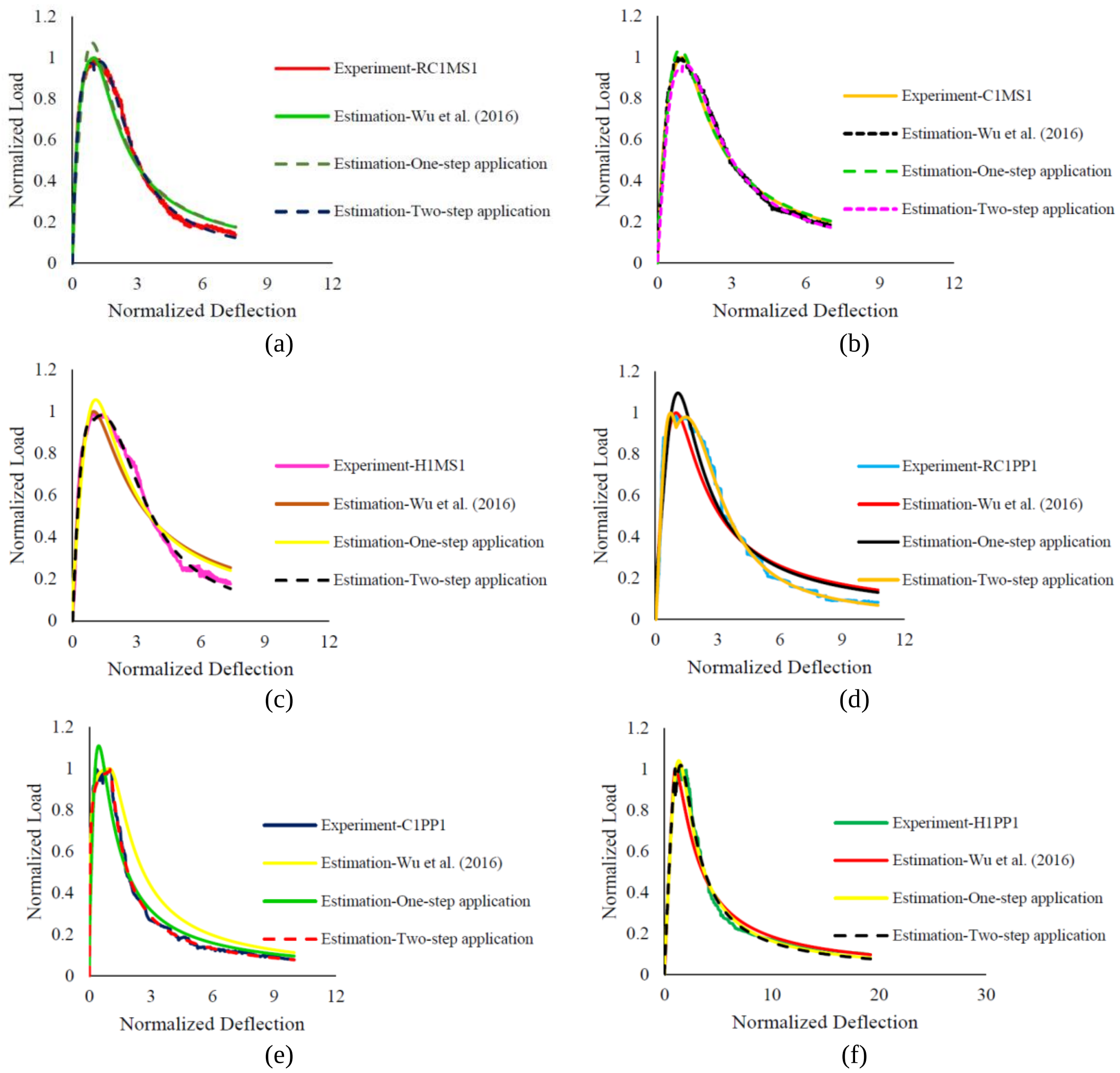

Fig. 15 Fitting curves of beam specimens based on the proposed equation and the work by Wu et al. (2016) (a) RC1MS1, (b) C1MS1, (c) H1MS1, (d) RC1PP1 (e) C1PP1, and (d) H1PP1

Table 6 Fitting parameters for flexural load-deflection curves according to the work by Wang and Xu (2002) and Wu *et al.* (2016)

Wang and Xu (2002)					
Sample ID	Parameter *a*	Parameter *b*	Parameter *c*	Parameter *d*	R^2
RC1MS1	181.9392	-12.8731	0.5324	0.4793	0.9809
C1MS1	133.9919	-7.5699	0.2370	0.5698	0.9863
H1MS1	130.0138	-10.1412	0.5308	0.2983	0.9858
RC1PP1	87.8595	-7.8382	0.1253	0.8416	0.9771
C1PP1	356.8675	-24.3390	3.8293	5.6380	0.9568
H1PP1	70.7667	-0.5310	-1.2495	2.1877	0.9883
Wu *et al.* (2016)					
	Parameter *a*	R^2	Parameter *b*	R^2	
RC1MS1	4.1510	0.9920	0.8300	0.9580	---
C1MS1	3.3040	0.9780	0.7790	0.9870	---
H1MS1	2.6850	0.9840	0.5320	0.9270	---
RC1PP1	2.5010	0.9410	0.6830	0.9220	---
C1PP1	23.5800	0.9820	0.9820	0.971	---
H1PP1	1.1820	0.9980	0.5420	0.9620	---

Table 7 Fitting parameters for the proposed equation to estimate normalized flexural load-deflection curves

One-step application					
Sample ID	Parameter a	Parameter b	Parameter c	Parameter d	R^2
RC1MS1	0.1824	1.2007	-0.6947	0.9903	0.9548
C1MS1	0.1255	1.4169	-0.5731	1.0660	0.9874
H1MS1	0.1186	1.2239	-0.4654	0.7428	0.9512
RC1PP1	0.1535	0.9098	-0.7428	0.7193	0.9418
C1PP1	0.1552	3.8282	-0.2994	4.0777	0.9547
H1PP1	0.0698	0.7502	-0.6742	0.5199	0.9900
Two-step application- Ascending branch					
RC1MS1	-0.0403	4.2190	1.9164	1.4000	0.9956
C1MS1	0.0100	1.7740	0.3696	1.2891	0.9962
H1MS1	-0.0553	2.8732	0.7310	1.1912	0.9906
RC1PP1	-0.0660	2.0297	-0.8944	2.0094	0.9752
C1PP1	-0.0202	28.2617	27.6510	-0.0318	0.9828
H1PP1	0.0168	1.0823	-0.2609	0.3561	0.9990
Two-step application- Descending branch					
RC1MS1	0.4306	0.1848	-0.6737	0.3308	0.9962
C1MS1	0.4289	0.3779	0.5817	0.4261	0.9978
H1MS1	0.7167	0.0341	-0.3625	0.1461	0.9952
RC1PP1	0.6139	0.0453	-0.4640	0.1744	0.9969
C1PP1	-1.3693	1.8810	-3.0560	2.6574	0.9970
H1PP1	-0.0194	0.5923	-0.7654	0.4440	0.9919

application approach and the work by Wu *et al*. (2016) as it is evident from the fitting curves and R^2 values over 0.90 given in Fig. 15 and Table 7, respectively.

6. Conclusions

This study presented mechanical tests on macro steel fibers combined with MS and PP fibers. Compression, tension and flexural tests were carried out on a large number of specimens. The following conclusions may be drawn from this study:

• For the obtained moduli of elastic in this study, available equations in the literature underestimate the modulus of elasticity hybrid steel fibers, mostly with a maximum margin of error of 10% and overestimate the moduli of elasticity of hybrid PP fibers, mostly at a maximum margin of also 10% (except for C1PP1 specimen).

• Cracking pattern was influenced by the replacement of PP fibers with MS fibers; irrespective of the type of macro fiber that the MS fiber was combined with, axial compression lead to crushing and cracking of concrete such that the integrity of the specimens was preserved and fibers prevented the severe spalling of concrete; in PP fibers, however, cracking was mainly characterized with longitudinal cracks along the height of cylinders with wider cracks.

• Among macro fibers, RC fibers had the best overall performance especially in flexure; flexural strengths equal to 37.71 MPa were obtained by the hybrid use of RC and MS fibers. Moreover, tensile strengths equal to 17.38 MPa were also obtained for the hybrid use of RC and PP fibers. However, the trend was not the same for compressive strength; H fibers had the highest cubic compressive strength (158 MPa) followed by C fibers (154 MPa) and RC fibers (141 MPa) when used with MS fibers.

• Deflections corresponding to peak loads were much higher (at least by 30% for C fibers) in specimens with MS fibers, rather than PP fibers.

• Using MS fibers instead of PP fibers greatly improved the toughness of the specimens. The difference was more pronounced for post-peak toughness values.

• Determination of toughness based on $L/150$ of the span as specified by ASTM C1609/1609M (2012) does not seem to reflect the toughness of the specimens. It is recommended that $L/50$ be used instead. However, more research is needed to further investigate the end deflection point.

• The methodology used in the numerical analyses successfully captured the flexural load-deflection response of the investigated beams.

• Fitting results based on the characteristics of the flexural load-deflection curve was established, having very good correlations with test results (R^2) 0.90.

Acknowledgments

The technical support received from Dr. Dobromil Pryl of Cervenka Consulting Company in preparation of the numerical model is greatly acknowledged.

References

Alsalman, A., Dang, C.N., Prinz, G.S. and Hale, W.M. (2017), "Evaluation of modulus of elasticity of ultra-high performance concrete", *Constr Build. Mater.*, **153**, 918-928. https://doi.org/10.1016/j.conbuildmat.2017.07.158.

Aslani, F., Nejadi, S. and Samali, B. (2014a), "Long-term flexural cracking control of reinforced self-compacting concrete one way slabs with and without fibres", *Comput. Concrete*, **14**(4), 419-443. http://dx.doi.org/10.12989/cac.2014.14.4.419.

Aslani, F., Nejadi, S. and Samali, B. (2014b), "Short term bond shear stress and cracking control of reinforced self-compacting concrete one way slabs under flexural loading", *Comput. Concrete*, **13**(6), 709-737. https://doi.org/10.12989/cac.2014.13.6.709.

Aslani, F., Nejadi, S. and Samali, B. (2015), "Instantaneous and time-dependent flexural cracking models of reinforced self-compacting concrete slabs with and without fibres", *Comput. Concrete*, **16**(2), 223-243. https://doi.org/10.12989/cac.2015.16.2.223.

ASTM C150/C150M (2017), Standard Specification for Portland Cement, ASTM International, West Conshohocken, PA.

ASTM C1609/C1609M (2012), Standard Test Method for Flexural Performance of Fiber-Reinforced Concrete (Using Beam With Third-Point Loading), ASTM International, West Conshohocken, PA.

ASTM C469/C469M (2014), Standard Test Method for Static Modulus of Elasticity and Poisson's Ratio of Concrete in Compression, ASTM International, West Conshohocken, PA.

ATENA (2016), Finite Element Software, ATENA Program Documentation, Theory and FRC User Manual, Cervenka Consulting, Prague, Czech Republic.

Banthia, N. and Gupta, R. (2004), "Hybrid fiber reinforced concrete (HyFRC): fiber synergy in high strength matrices", *Mater. Struct.*, **37**(10), 707-716. https://doi.org/10.1007/BF02480516.

Brandt, A.M. (2005), *Cement-based Composites: Materials, Mechanical Properties and Performance*, CRC Press.

Farzam, M. and Sadaghian, H. (2018), "Mechanical model for punching shear capacity of rectangular slab-column connections", *Struct. Concrete*, **19**(6), 1983-1991. https://doi.org/10.1002/suco.201700213.

Farzam, M., Sadaghian, H. and Khodadade, G. (2019), "Shear behaviour of elongated rectangular wall–footing connections under eccentric loads", *Mag. Concrete Res.*, **71**(1), 43-54. https://doi.org/10.1680/jmacr.17.00378.

Ganesan, N., Sahana, R. and Indira, P.V. (2017), "Effect of hybrid fibers on tension stiffening of reinforced geopolymer concrete", *Adv. Concrete Constr.*, **5**(1), 075. http://dx.doi.org/10.12989/acc.2017.5.1.075.

GID (2015), International Centre for Numerical Methods in Engineering (CIMNE), Spain.

Graybeal, B.A. (2007), "Compressive behavior of ultra-high-performance fiber-reinforced concrete", *ACI Mater. J.*, **104**(2), 146.

Graybeal, B.A. and Stone, B. (2012), "Compression response of a rapid-strengthening ultra-high performance concrete formulation", US Department of Transportation, Federal Highway Administration.

Haber, Z.B., De la Varga, I., Graybeal, B.A., Nakashoji, B. and El-Helou, R. (2018), "Properties and behavior of UHPC-class materials (No. FHWA-HRT-18-036)", Federal Highway Administration, Office of Infrastructure Research and Development, United States.

Halvaei, M., Jamshidi, M. and Latifi, M. (2016), "Investigation on pullout behavior of different polymeric fibers from fine aggregates concrete", *J. Indust. Text.*, **45**(5), 995-1008. https://doi.org/10.1177/1528083714551437.

Hsie, M., Tu, C. and Song, P.S. (2008), "Mechanical properties of polypropylene hybrid fiber-reinforced concrete", *Mater. Sci. Eng.: A*, **494**(1-2), 153-157. https://doi.org/10.1016/j.msea.2008.05.037.

JSCE-SF4 III, P. (1984), Method of Tests for Steel Fiber Reinforced Concrete, Concrete Library of JSCE, The Japan Society of Civil Engineers.

Kandekar, S.B. and Talikoti, R.S. (2020), "Torsional behaviour of reinforced concrete beams retrofitted with aramid fiber", *Adv. Concrete Constr.*, **9**(1), 1-7. https://doi.org/10.12989/acc.2020.9.1.001.

Kang, S.T., Choi, J.I., Koh, K.T., Lee, K.S. and Lee, B.Y. (2016), "Hybrid effects of steel fiber and microfiber on the tensile behavior of ultra-high performance concrete", *Compos. Struct.*, **145**, 37-42. https://doi.org/10.1016/j.compstruct.2016.02.075.

Kannam, P. and Sarella, V.R. (2018), "A study on validation of shear behaviour of steel fibrous SCC based on numerical modelling (ATENA)", *J. Build. Eng.*, **19**, 69-79. https://doi.org/10.1016/j.jobe.2018.05.003.

Kim, D.J., Park, S.H., Ryu, G.S. and Koh, K.T. (2011), "Comparative flexural behavior of hybrid ultra high performance fiber reinforced concrete with different macro fibers", *Constr. Build. Mater.*, **25**(11), 4144-4155. https://doi.org/10.1016/j.conbuildmat.2011.04.051.

Kollmorgen, G.A. (2004), "Impact of age and size on the mechanical behavior of an ultra high performance concrete", Doctoral Dissertatio, Michigan Technological University.

Korea Concrete Institute (KCI) (2007), Concrete Design Code and Commentary, Kimoondang Publishing Co., Seoul, Republic of Korea.

Li, B., Chi, Y., Xu, L., Shi, Y. and Li, C. (2018), "Experimental investigation on the flexural behavior of steel-polypropylene hybrid fiber reinforced concrete", *Constr. Build. Mater.*, **191**, 80-94. https://doi.org/10.1016/j.conbuildmat.2018.09.202.

Mansouri, I., Shahheidari, F.S., Hashemi, S.M.A. and Farzampour, A. (2020), "Investigation of steel fiber effects on concrete abrasion resistance", *Adv. Concrete Constr.*, **9**(4), 367-374. https://doi.org/10.12989/acc.2020.9.4.367.

Mazloom, M., Karimpanah, H. and Karamloo, M. (2020), "Fracture behavior of monotype and hybrid fiber reinforced self-compacting concrete at different temperatures", *Adv. Concrete Constr.*, **9**(4), 375-386. https://doi.org/10.12989/acc.2020.9.4.375.

Mezquida-Alcaraz, E.J., Navarro-Gregori, J., Lopez, J.A. and Serna-Ros, P. (2019), "Validation of a non-linear hinge model for tensile behavior of UHPFRC using a Finite Element Model", *Comput. Concrete*, **23**(1), 11-23. https://doi.org/10.12989/cac.2019.23.1.011.

Nguyen, D.L., Ryu, G.S., Koh, K.T. and Kim, D.J. (2014), "Size and geometry dependent tensile behavior of ultra-high-performance fiber-reinforced concrete", *Compos. Part B: Eng.*, **58**, 279-292. https://doi.org/10.1016/j.compositesb.2013.10.072.

Park, S.H., Kim, D.J., Ryu, G.S. and Koh, K.T. (2012), "Tensile behavior of ultra high performance hybrid fiber reinforced concrete", *Cement Concrete Compos.*, **34**(2), 172-184. https://doi.org/10.1016/j.cemconcomp.2011.09.009.

Pourbaba, M., Asefi, E., Sadaghian, H. and Mirmiran, A. (2018a), "Effect of age on the compressive strength of ultra-high-performance fiber-reinforced concrete", *Constr. Build. Mater.*, **175**, 402-410. https://doi.org/10.1016/j.conbuildmat.2018.04.203.

Pourbaba, M., Joghataie, A. and Mirmiran, A. (2018b), "Shear behavior of ultra-high performance concrete", *Constr. Build. Mater.*, **183**, 554-564. https://doi.org/10.1016/j.conbuildmat.2018.06.117.

Pourbaba, M., Sadaghian, H. and Mirmiran, A. (2019a), "A comparative study of flexural and shear behavior of ultra-high-performance fiber-reinforced concrete beams", *Adv. Struct. Eng.*, **22**(7), 1727-1738. https://doi.org/10.1177/1369433218823848.

Pourbaba, M., Sadaghian, H. and Mirmiran, A. (2019b), "Flexural response of UHPFRC beams reinforced with steel rebars", *Adv. Civil Eng. Mater.*, **8**(3), 411-430. https://doi.org/10.1520/ACEM20190129.

Raj, S.D., Ganesan, N. and Abraham, R. (2020), "Role of fibers on the performance of geopolymer concrete exterior beam column joints", *Adv. Concrete Constr.*, **9**(2), 115-123. https://doi.org/10.12989/acc.2020.9.2.115.

Rasoolinejad, M. and Bažant, Z.P. (2019), "Size effect of squat shear walls extrapolated by microplane model M7", *ACI Struct. J.*, **116**(3), 75-84.

Sadaghian, H. and Farzam, M. (2019), "Numerical investigation on punching shear of RC slabs exposed to fire", *Comput. Concrete*, **23**(3), 217-233. https://doi.org/10.12989/cac.2019.23.3.217.

Sadaghian, H. and Farzam, M. (2019), "Numerical investigation on punching shear of RC slabs exposed to fire", *Comput. Concrete*, **23**(3), 217-233. https://doi.org/10.12989/cac.2019.23.3.217.

Sahoo, D.R., Solanki, A. and Kumar, A. (2014), "Influence of steel and polypropylene fibers on flexural behavior of RC beams", *J. Mater. Civil Eng.*, **27**(8), 04014232. https://doi.org/10.1061/(ASCE)MT.1943-5533.0001193.

Şanal, İ. (2018), "Performance of macrosynthetic and steel fiber–reinforced concretes emphasizing mineral admixture addition", *J. Mater. Civil Eng.*, **30**(6), 04018101.

Sharma, R. and Bansal, P.P. (2019), "Efficacy of supplementary cementitious material and hybrid fiber to develop the ultra high performance hybrid fiber reinforced concrete", *Adv. Concrete Constr.*, **8**(1), 21-31. https://doi.org/10.12989/acc.2019.8.1.021.

Smarzewski, P. (2017), "Effect of curing period on properties of steel and polypropylene fibre reinforced ultra-high performance concrete", *IOP Conf. Ser.: Mater. Sci. Eng.*, **245**(3), 032059.

Soe, K.T., Zhang, Y.X. and Zhang, L.C. (2013), "Material properties of a new hybrid fibre-reinforced engineered cementitious composite", *Constr. Build. Mater.*, **43**, 399-407. https://doi.org/10.1016/j.conbuildmat.2013.02.021.

Sridhar, R. and Prasad, R. (2019), "Damage evaluation of RC beams strengthened with hybrid fibers", *Adv. Concrete Constr.*, **8**(1), 9-19. https://doi.org/10.12989/acc.2019.8.1.009.

Swamy, R.N. (1985), "High-strength concrete-material properties and structural behavior", *Spec. Publ.*, **87**, 119-146.

Wang, L.M. and Xu, S.L. (2002), "Characteristic curve of concrete and fiber reinforced concrete", *J. Dalian Univ. Technol.*, **42**(5), 580-585.

Wang, P.T., Shah, S.P. and Naaman, A.E. (1978), "Stress-strain curves of normal and lightweight concrete in compression", *J. Proc.*, **75**(11), 603-611.

Wee, T.H., Chin, M.S. and Mansur, M.A. (1996), "Stress-strain relationship of high-strength concrete in compression", *J. Mater. Civil Eng.*, **8**(2), 70-76. https://doi.org/10.1061/(ASCE)0899-1561(1996)8:2(70).

Wu, Z., Shi, C., He, W. and Wu, L. (2016), "Effects of steel fiber content and shape on mechanical properties of ultra high performance concrete", *Constr. Build. Mater.*, **103**, 8-14. https://doi.org/10.1016/j.conbuildmat.2015.11.028.

Xu, L., Huang, L., Chi, Y. and Mei, G. (2016), "Tensile behavior of steel-polypropylene hybrid fiber-reinforced concrete", *ACI Mater. J.*, **113**(2), 219-229.

Yan, G. (2005), "Study on failure criterion and constitutive relationship of 200 MPa reactive powder concrete (RPC200)", Doctoral Dissertation, Beijing Jiaotong University.

Yoo, D.Y., Kim, M.J., Kim, S.W. and Park, J.J. (2017b), "Development of cost effective ultra-high-performance fiber-reinforced concrete using single and hybrid steel fibers", *Constr. Build. Mater.*, **150**, 383-394. https://doi.org/10.1016/j.conbuildmat.2017.06.018.

Yoo, D.Y., Kim, S., Park, G.J., Park, J.J. and Kim, S.W. (2017a), "Effects of fiber shape, aspect ratio, and volume fraction on flexural behavior of ultra-high-performance fiber-reinforced cement composites", *Compos. Struct.*, **174**, 375-388. Get rights and content.

Yoo, D.Y., Kim, S.W. and Park, J.J. (2017c), "Comparative flexural behavior of ultra-high-performance concrete reinforced with hybrid straight steel fibers", *Constr. Build. Mater.*, **132**, 219-229. https://doi.org/10.1016/j.conbuildmat.2016.11.104.

Zhenghai, G. (1997), *Strength and Deformation of Concrete: Test Basis and Constitutive Relation*.

JK